RESEARCH



Novel strut-based mechanical analysis: flow stress determination of electron beam melt (EBM) lattice structures

Muhammad Arslan Bin Riaz^{1,2} · Hacer İrem Erten¹ · Mustafa Güden¹

Received: 16 April 2025 / Accepted: 16 September 2025 © The Author(s), under exclusive licence to Springer Nature Switzerland AG 2025

Abstract

In modeling lattices, the material flow stress equation, such as the Johnson and Cook (JC) equation, is usually determined from the mechanical tests conducted on bulk, relatively large test size specimens which were manufactured using the same process parameters with the lattices. However, the flow stresses of struts were shown in several studies to be significantly lower than those of large size test specimens. To overcome this discrepancy, a novel approach that combined the strut compression test, the strut double shear test (DST) and the numerical model of the strut DST using the JC equation was proposed. The study confirmed that the flow stress determined from the machined bulk tension test specimens overestimated the experimental compression stress–strain behavior of a body centered cubic (BCC) Ti6Al4V lattice. The flow stress parameters determined from the compression stress–strain curves of the as-printed strut specimens, on the other side, showed the best match to the experimental compression stress–strain behavior of the BCC lattice. The fidelity of the determined parameters of the JC equation was further verified with the experimental and numerical DSTs. It was also shown that the numerical iterations of DST model could be used for the fine-tuning the flow stress parameters.

Keywords Double shear test · Constitutive modeling · Lattice structures · Additive manufacturing · Struts

1 Introduction

Additive manufacturing (AM) has enabled researchers to design, manufacture and test various kinds of structures that were not possible previously through conventional techniques. The structured parts obtained from the AM technique in many cases require less additional post-processing steps than their conventional counterparts. The AM produced parts rely on the layer-by-layer manufacturing technique in which a design is divided into finite slices which are then realized through the melting of powder with a heat source. Electron-beam melting (EBM) is a subcategory of

Mustafa Güden mustafaguden@iyte.edu.tr

Muhammad Arslan Bin Riaz arslanbinriaz@gmail.com

Published online: 25 September 2025

Hacer İrem Erten erteniremm@gmail.com

- Izmir Institute of Technology, Izmir, Turkey
- Additive Manufacturing Technology Application and Research Center, Gazi University, Ankara, Turkey

AM in which the material is melted inside the vacuum chamber with the help of high powered electron beam. The powder-beam interaction results in the melting of the powder resulting in a strong bond between the layers. In metallic materials, the EBM of lattice structures is mostly focused on titanium, aluminum, iron-based alloys and nickel alloys [1]. Ti6Al4V (Ti64) is among the widely investigated material that provides the best strength-to-weight ratio among the alloys currently being produced using EBM technology [2, 3]. The microstructure of EBM produced Ti64 is mainly composed of the $\alpha + \beta$ lamellar microstructure, giving it a high strength and an elongation to failure [4]. Ti64-based lattices have been reviewed extensively and have applications in aerospace, protective equipment, military, automobile, etc., where the high strength-to-weight ratio is an important prerequisite [5].

One of the most important relations while studying lattices is a power law correlation found between the relative density and strength proposed by Gibson and Ashby model [6, 7]. Several researchers have investigated the tensile, compressive and fatigue properties of Ti64 lattices and found a correlation between the strut size or cell wall thickness to the mechanical response [8]. The printing of lattices in the



ranges of several micrometers to millimeters often results in imperfections in the final produced shape including porosities, lack of fusion, irregular surface and many others [9]. These imperfections have significant effect on the deformation behavior and energy absorption capacity. Literature show that these imperfections can be somehow avoided through carefully selecting the process parameters such as the melt strategy, layer thickness and energy density [10]. In addition, the waviness of the as-designed cylindrical struts has also been viewed in a few studies, and it was shown that the printing direction has a huge effect on efficiency in terms of capturing the full design geometry [11].

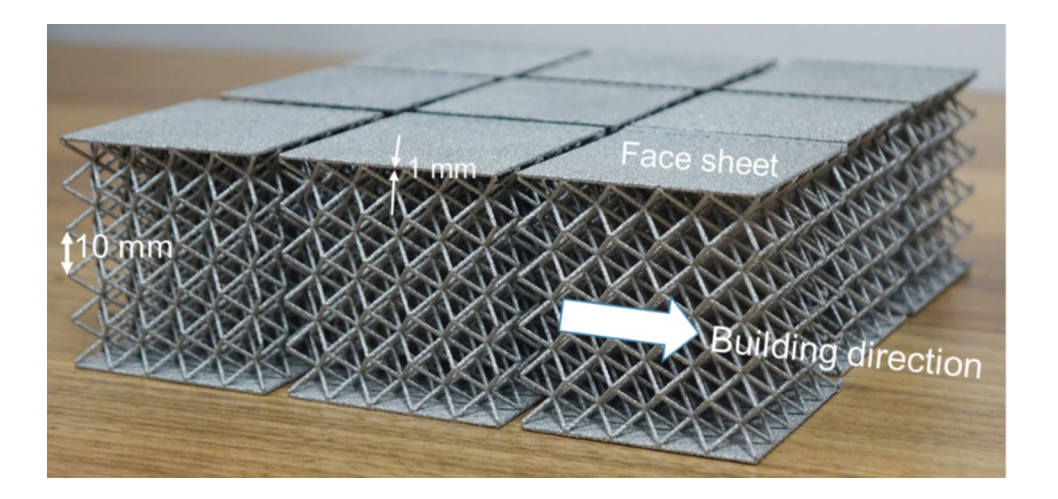
In modeling lattice structure (LS), the material constitutive equations including the flow stress and damage are usually determined from the mechanical tests conducted on bulk, large size test specimens which are manufactured using the same process parameters with lattices. However, the flow stresses of struts were found significantly lower than those of large size bulk test specimens [12–14]. This discrepancy may result from the variations in (a) residual stresses, (b) microstructures, and (c) surface roughness between large and small-size test specimens. To obtain representative material models of LSs, micro-tensile and in situ micro-tensile tests on individual or multiple struts were further applied [15–18]. Another approach is to calibrate the numerical models with the experiments [19]. All these are noted to increase the physical-testing and computational efforts. The challenges encountered when deploying EBM lattice structures in real-world robust applications must be carefully analyzed and resolved, in addition to manufacturing considerations. The present work aims to address the challenges related to the application of EBM produced LSs by providing a simple alternative test and numerical method that eliminates extensive testing and computational requirements by directly testing the struts under compression and in a miniaturized double shear test (DST) apparatus. DST's with different test assemblies have been used previously to

assess the mechanical performance of metals and ceramics [20, 21]. A relatively recent study published by Meyer and Halle [22] also emphasizes the importance of using shear tests in several industrial applications and impact processes. They have also pointed out that the DST can be employed for the evaluation of flow behavior of the material and can be used for higher strain-rate studies [23]. The DST is easy to conduct and simulate, resulting in efficient workflow and is found to be useful in situations where extensive testing equipment or computational devices are not available. In this study, the constitutive equation obtained from the individual strut compression test was dually verified with the DST's simulations and afterwards were used to simulate the mechanical behavior of a bigger lattice. It also explains the inaccuracies while obtaining a constitutive equation through bulk samples.

2 Experimental methodology

The body centered cubic (BBC) lattices with face sheets were printed in an ARCAM EBM A2X device using Ti64 ELI Grade 5 spherical powder of 30–110 µm. The strut samples for DST were prepared by cutting the struts from these as-printed BBC sandwich lattices using a diamond saw under continuous flow of water. The EBM process parameters used to fabricate the BCC lattices were: the beam speed was 40.5 m s⁻¹; the hatch depth was 70 µm; scanning layer thickness was 90 μ m; the scan speed was 4530 mm s⁻¹; the hatch distance was 200 µm and the pre-heat temperature was 700 °C. A straight contour of scanning was used for printing the samples. The face sheets on both the top and bottom of the sandwich BCC design were 1 mm in thickness and the building direction is parallel to the face sheets as seen in Fig. 1. The lattices had $5 \times 5 \times 5$ cells (total 125 cells) with a cell length of 10 mm and strut thickness of 1 mm. Bulk cylindrical samples in 10 mm diameter and 80 mm in

Fig. 1 The pictures of the fabricated BCC sandwich lattices, building direction and dimensions of the cells and face sheets

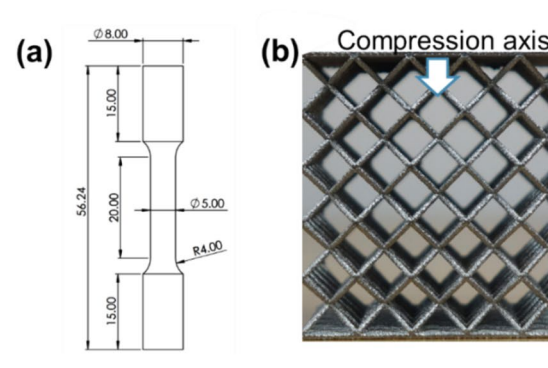




length (building direction through the long axis) were also fabricated using the same process parameters with the lattice to determine bulk specimen material flow stress model by performing tension tests.

The mechanical tests on the machined bulk tension specimens, as-received BCC lattices and cut-strut specimens were conducted in a Shimadzu 300 kN test machine with a video extensometer attachment. The larger tension specimens were in 20 mm in gage length and 5 mm in gage diameter as depicted in Fig. 2a. Smaller size machined specimens, 14 mm in gage length and 2.5 mm in gage diameter, were also tested to the see the specimen size effect. The compression load was applied to the upper face sheet of the BCC lattices as seen in Fig. 2b. The micro-scale compression tests were employed on small-size cylindrical struts, 1 mm in diameter and 1.5 mm in length, to find the constitutive equations (Fig. 2c). These strut specimens were cut again from the as-received BCC lattice sandwich structures for DSTs. In tension and compression tests, the strain rate was 1×10^{-3} s⁻¹. The pictures and technical drawings of DST apparatus are shown in Fig. 3a-d. The parts of the apparatus were machined from a tool steel according to the military standard (MIL-STD-1312-13/NASM 1312-12). The apparatus is composed of two parts: the upper moving part and the bottom stationary part (Fig. 3a). The compression load is applied from the upper part and the strut is placed to the bottom part as seen in Fig. 3b. The diameter of the strut specimen is 1 mm and the length is 6.67 mm. The load is applied from the upper part while the bottom part remains stationary. The applied force until about shear failure of the test specimen was recorded and the displacement was measured both from the machine stroke and using a video extensometer. The height and width of the bottom stationary part and upper part are 10 mm (Fig. 3c and d) and the lower end of the upper part moves freely in the bottom part (1.9 mm). The cross-head speed was 0.035 mm s^{-1} .

Fig. 2 The pictures of a larger bulk tension (dimensions in mm), b BCC lattice and cs small-size strut compression test specimen



Strut Upper test platen specimen

3 Numerical simulations

The compression of the BCC lattice and DST on the strut specimens were modeled using the Johnson–Cook (JC) flow stress and damage model. The flow stress σ_y in the JC flow stress model is [24]:

$$\sigma_{y} = \left(A + B\varepsilon_{ep}^{n}\right) \left[1 + cIn(\dot{\varepsilon}^{*})\right] \left[1 - (T^{*})^{m}\right],\tag{1}$$

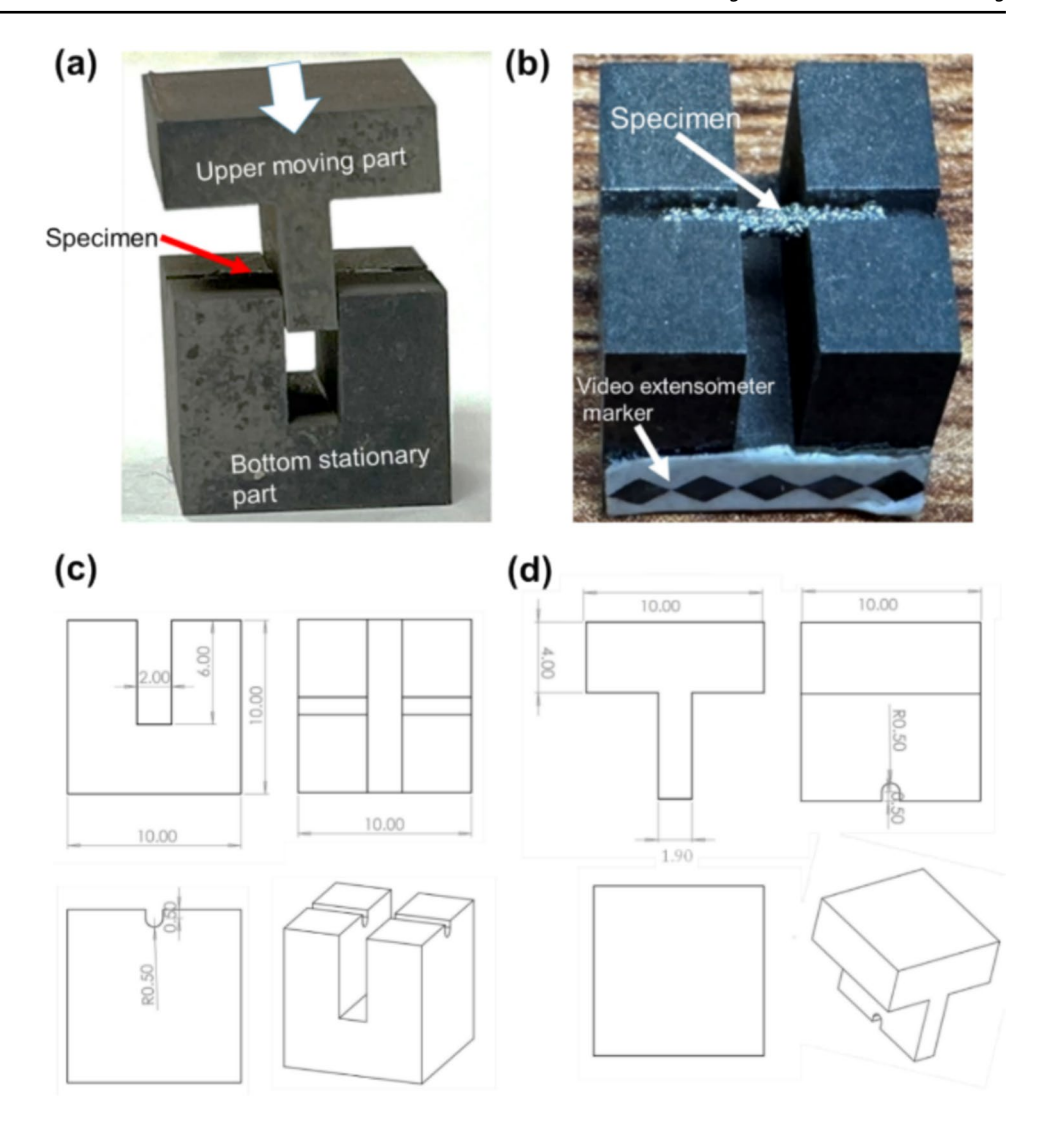
where A, B, n, c, and m are sequentially the yield stress, hardening modulus, strain hardening coefficient, strain rate sensitivity and thermal softening parameters, $\dot{\varepsilon}^* = \left(\frac{\dot{\varepsilon}_{ep}}{\dot{\varepsilon}_0}\right)$; where ε_{ep} , $\dot{\varepsilon}_{ep}$ and $\dot{\varepsilon}_0$ are sequentially the equivalent plastic strain, strain rate and reference strain rate; $T^* = \left(\frac{T - T_r}{T_m - T_r}\right)$; where T is the temperature, T_m is the melting temperature, and T_r is the reference or room temperature. The plastic strain at fracture (ε_{pf}) in the JC damage model is [25]:

$$\varepsilon_{pf} = \left[D_1 + D_2 e^{D_3 \sigma^*}\right] \left[1 + D_4 \ln(\varepsilon^*)\right] \left[1 + D_5 T^*\right],\tag{2}$$

where D_1 – D_5 are the parameters determined experimentally and σ^* is the stress triaxiality, which is $\frac{\sigma_h}{\sigma_e}$; where σ_h is the hydrostatic stress and σ_e is the equivalent stress. The damage model parameters used in the lattice deformation and DST models in the present study were taken from a similar EBM-Ti64 alloy given in the reference [14]: D_1 =0.1, D_2 =0.142 and D_3 =1.5. These damage parameters at the reference strain rate of 1×10^{-3} s⁻¹ and the reference temperature of 25 °C were shown to well present the failure of the BCC lattices with 2 mm strut diameter.

Commercial software LS-DYNA was used to simulate quasi-static ($1 \times 10^{-3} \text{ s}^{-1}$) compression tests of lattices. Figure 4 shows the 125-cell (5-cells/edge) of the compression model. The moving and stationary plates were modeled with constant stress solid elements of the material definition (E = 210 GPa, = 7800 kg m⁻³, and the Poisson's ratio = 0.33). One-point nodal pressure tetrahedral elements (solid 164) were used to model the struts and face sheets. The mesh size was determined 0.25 mm size after a detailed mesh sensitivity analysis. The hourglass rigidity definition

Fig. 3 The pictures of DST apparatus: a upper and bottom part and b bottom part with a strut specimen and the technical drawings and dimensions (in mm) of c the bottom and d upper part



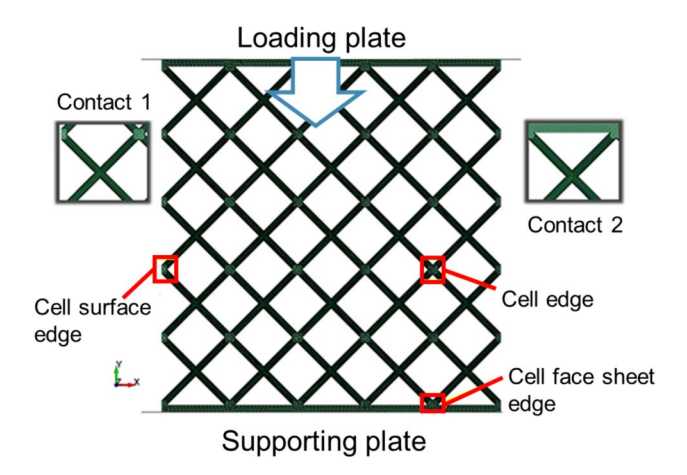


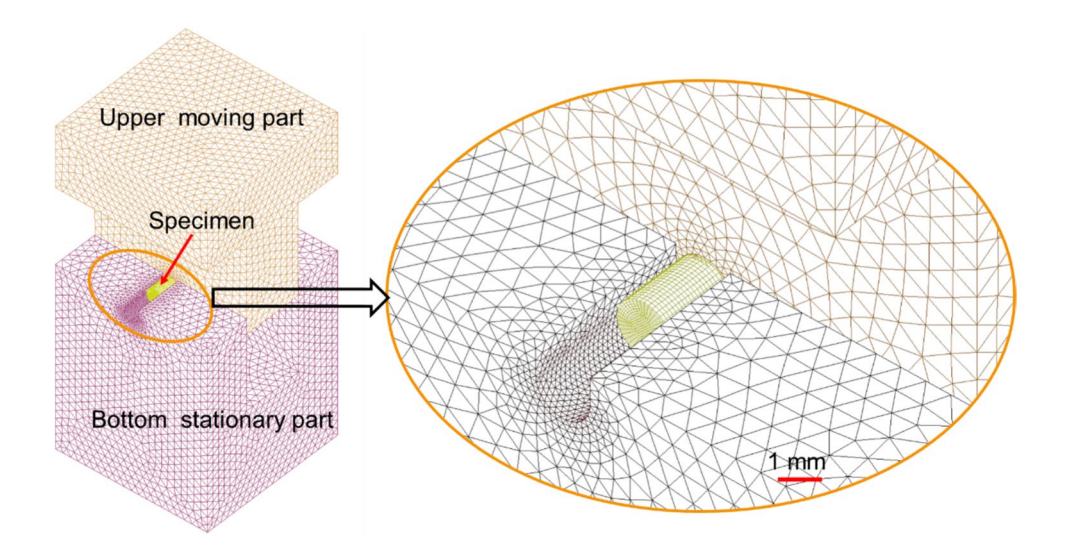
Fig. 4 Lattice compression test model

of Flanagan–Belytschko was used. The contact was defined as SINGLE_SURFACE_CONTACT for the struts (Contact 1 in Fig. 4), while the SURFACE_TO_SURFACE_CONTACT was defined for rigid compression platens and lattices (Contact 2 in Fig. 4). The distinct features such as the cell edge where struts meet, cell surface edge and the cell surface face sheets corner can also be seen in the figure. Significant mass scaling was required to achieve a correct solution in less time. The coefficients of static dynamic friction were 0.3 and 0.2, respectively.

The model of the DST apparatus with a strut specimen is shown in Fig. 5. The upper moving parts and bottom stationary part were modeled using approximately 0.3 million constant stiff solid elements (E = 210 GPa, = 7800 kg m⁻³, and Poisson's ratio = 0.33). A fine mesh is used near the contact of specimen and rigid parts as seen in Fig. 5. The specimen 6.67 mm in length and 1 mm in diameter was modeled using 42,000 elements with a mesh size of 0.035 mm. The contact between specimen and steel apparatus was defined



Fig. 5 DST model



by the SURFACE_TO_SURFACE_CONTACT. The velocity of the upper moving part in the model was the same as the tests. The static and dynamic friction coefficients values remained unchanged.

4 Results and discussion

Figure 6a shows the surface quality of the as-built strut and the front view of the as-built lattices with face sheets. Partially melted powder particles can be seen attached to the surface as marked in Fig. 6b. As the lattice sample is being built inside the chamber, the struts are not only inclined (overhanging) at an angle to the build direction, but they are also moving inwards and outwards from the

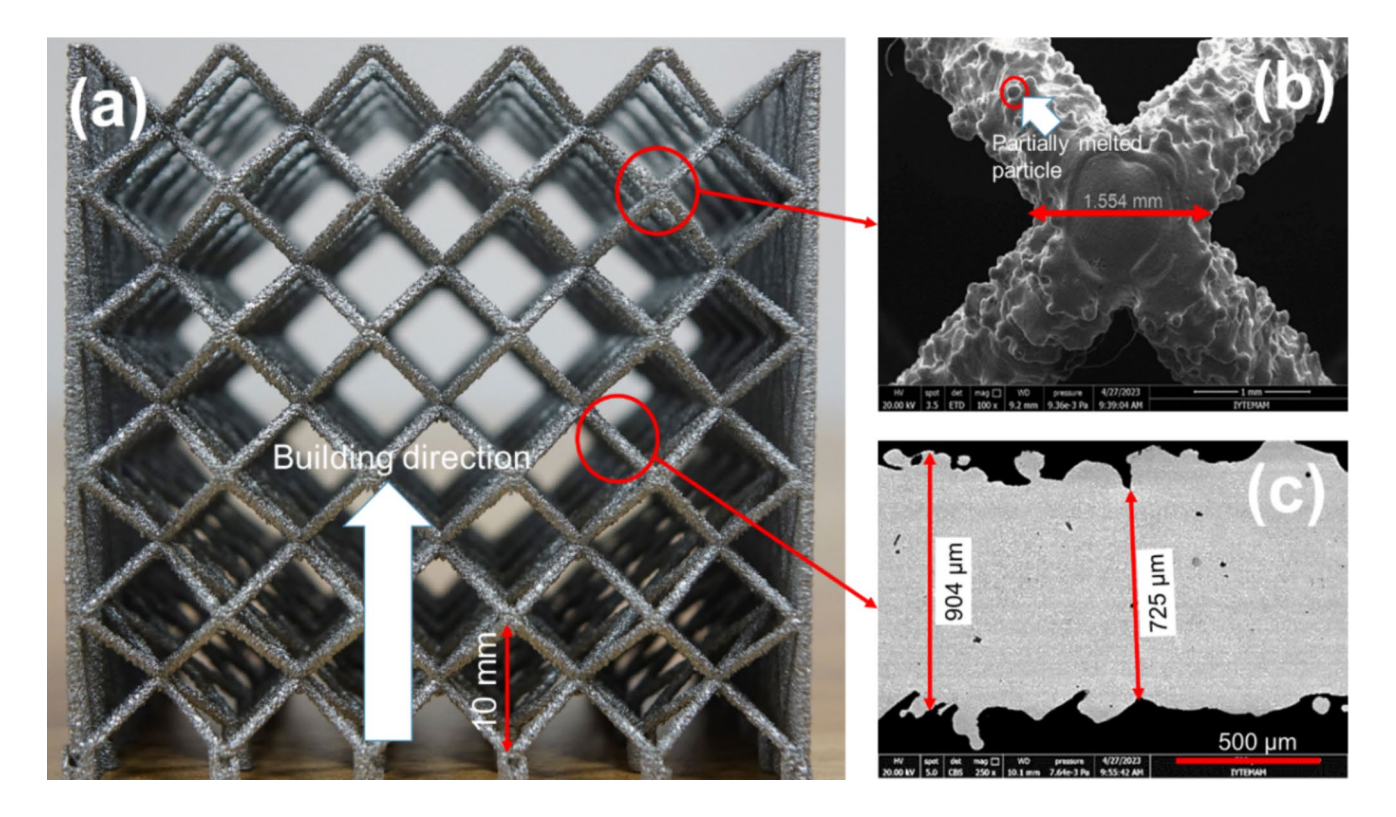


Fig. 6 A picture of a BCC lattice, b cell edge corner and c strut cross-section

viewing plane making it difficult for the printer to follow the contours perfectly which results in a rough surface. Also, it has been shown in previous research that the printing of thin features always results in imperfections as the mass error (with as-designed CAD design) keeps increasing moving from bigger diameter cylinders to smaller ones [26]. From the polished cross-section of a strut, it becomes evident that the as-built design is far from the as-designed CAD geometry with pointy corners and protrusion of the partially melted powder particles attached to the surface. Figure 6c shows the thickness of the strut from the cross section as in some areas the 1 mm designed strut is reduced to 725 µm with the pores inside as also seen in previous studies [26]. The presence of cracks or porosities inside or at the surface result in the deterioration of mechanical performance. For an elliptical pore, the maximum stress at the tip (σ_{max}) -Inglis solution 1913 [27], is given as:

$$\sigma_{\text{max}} = \sigma \left(1 + 2\sqrt{\frac{a}{\rho}} \right). \tag{3}$$

Here, ρ is the radius of curvature and a is the radius of the pore of the tip of porosity and σ is the uniform tensile stress. The ratio $\sqrt{\frac{a}{\rho}}$ plays a crucial role as the ellipse becomes more elongated resulting in a higher maximum stress. The addition of such porosities and irregularities significantly reduces the mechanical properties especially the energy absorption of lattice as most of the struts when loaded, go through a mix of tensile, compression and shear failure. In addition, surface roughness, especially with sharp features at short distances, leads to stress concentrations. These stress concentrations can initiate cracks and plastic deformation, reducing the mechanical strength [28]. Studies also show that the overhanging designs result in porosities inside the structure which coalescence with the surface features resulting in reduced mechanical performance [29]. All these factors point to a fact that the thick sectioned printed samples

cannot effectively represent the mechanical performance of a lattice structure having thin-walled cylinders [14].

The quasi-static tensile engineering tensile stress-strain and true stress-true plastic strain curves of the larger and smaller size specimens are shown in Fig. 7a and b, respectively. The larger size specimens (5 mm in gage diameter) exhibit higher flow stresses than those of the smaller size specimens (2.5 mm in gage diameter). The yield strengths of 5 mm and 2.5 mm size specimens are 1000 and 870 MPa and the ultimate tensile strengths 1115 and 1000 MPa on the average, respectively. The determined JC parameters of A, B and n are also tabulated in Fig. 7b. The strut compression true stress-plastic true strain curves and the fitted JC parameters are further shown in Fig. 7b for comparison. The yield strength of the strut is lower than those of the 2.5- and 5-mm diameter tension specimens. These results clearly indicate that as the diameter of the test specimen decreases the flow stress parameters A and B also decrease.

The experimental (3 tests) and numerical force–displacement curves of DST are shown in Fig. 8a. As is noted in the same figure that experimental and numerical strut samples show yielding before shear failure. The experimental test samples also show significant variations in the force values after yielding but if we compare the results of flow stress obtained from the strut compression, it is closer to the experiments whereas the 5 mm and 2.5 mm diameter tension test specimens yields higher forces than the experimental force values. It was also noted that the experimental and numerical DST samples fail almost at a similar final strain, ~0.11. This also proves the validity of the used damage model $(D_1 = 0.1, D_2 = 0.142, D_3 = -1.5)$. The constitutive equations obtained from the bigger and smaller sized bulk specimen also show an over estimation in the overall material strength and overlook the irregularities on the surface of the as-built samples. After the numerical and experimental validation of the constitutive equation on a single strut, the constitutive model was tested for the bigger 5×5×5 BCC lattice. Figure 8b shows the experimental and numerical compression

Fig. 7 The quasi-static a engineering tensile stress-strain curves of larger and smaller specimens and b true stress-true plastic strain tensile curves of the larger and smaller size specimens and true stress-true plastic strain compression curve of strut

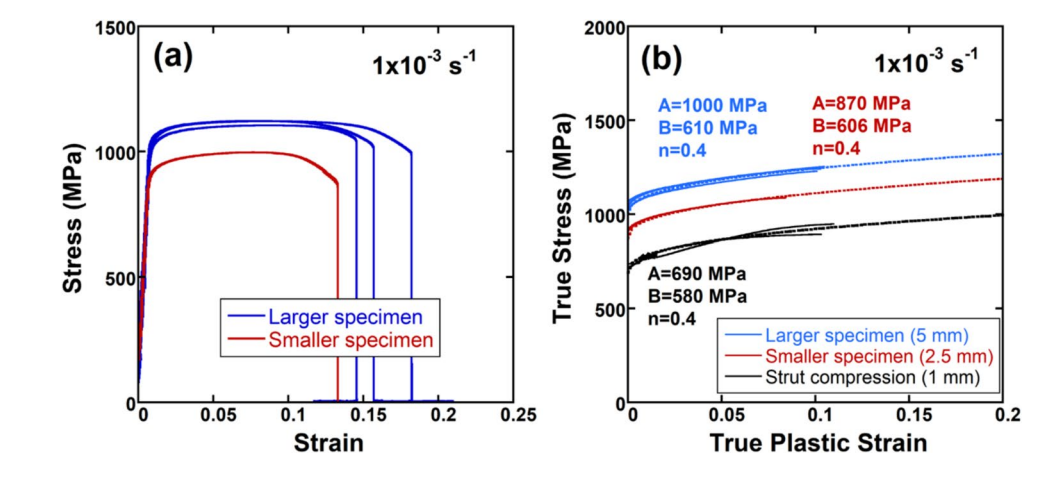




Fig. 8 Experimental and numerical **a** strut DST force—displacement curves and **b** lattice compression stress—strain curves

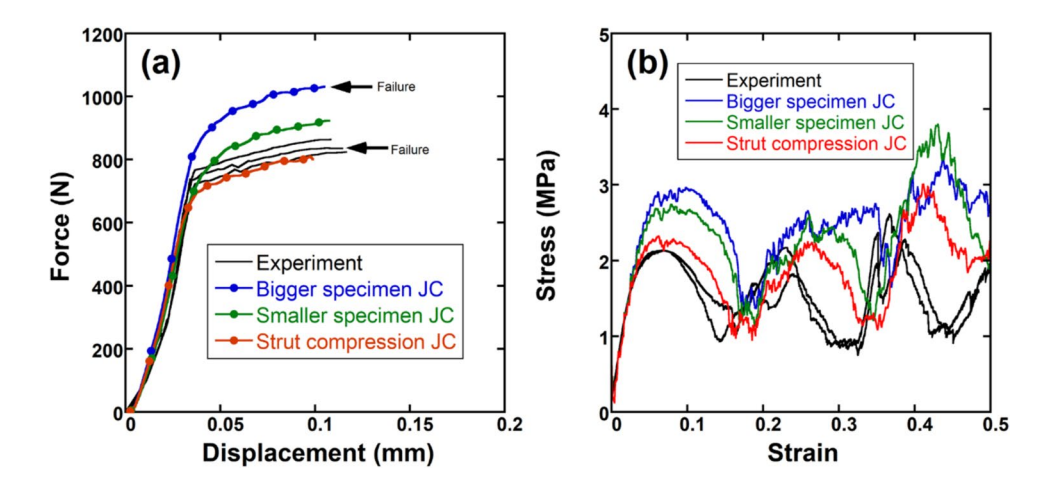


Table 1 Comparison of mechanical properties of different flow stress models

| Material model | 1 st peak stress | 1 st peak stress% diff to experiments | Densification strain ϵ_D | EA (J) |
|---------------------|------------------|---------------------------------------|-----------------------------------|--------|
| Experiments average | 2.12 MPa | - | 0.667 | 189.32 |
| Big bulk model | 2.95 MPa | 28.5 | 0.721 | 308.86 |
| Small bulk model | 2.72 MPa | 22.4 | 0.659 | 270.29 |
| DST model | 2.27 MPa | 7 | 0.679 | 204.51 |

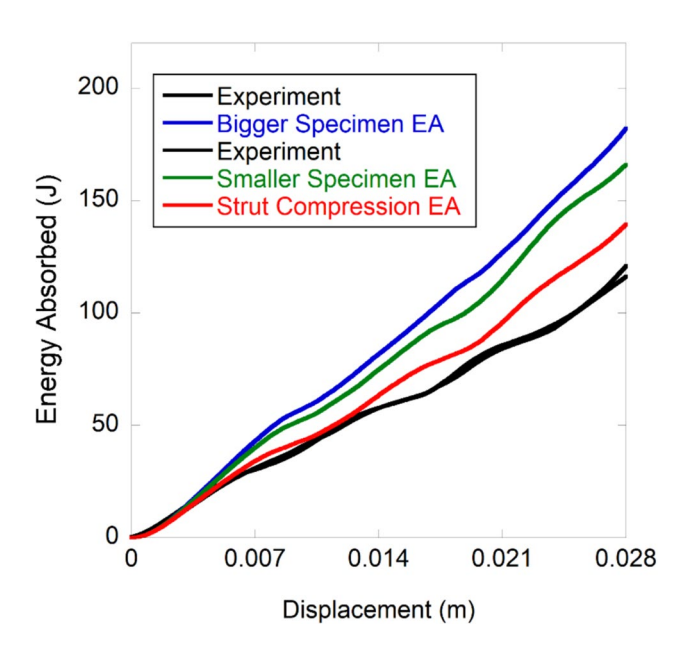


Fig. 9 Energy absorption comparison (experiments vs numerical models)

stress-strain graphs of the BCC lattices. The JC flow stress equations parameters determined from the smaller and bigger bulk specimens overestimate the stress values of the experimental tests as seen in the previous tests. The strut compression (DST verified) model showed a comparable stress behavior to the experimental stresses (peaks and valleys). Mechanical properties comparison of different models

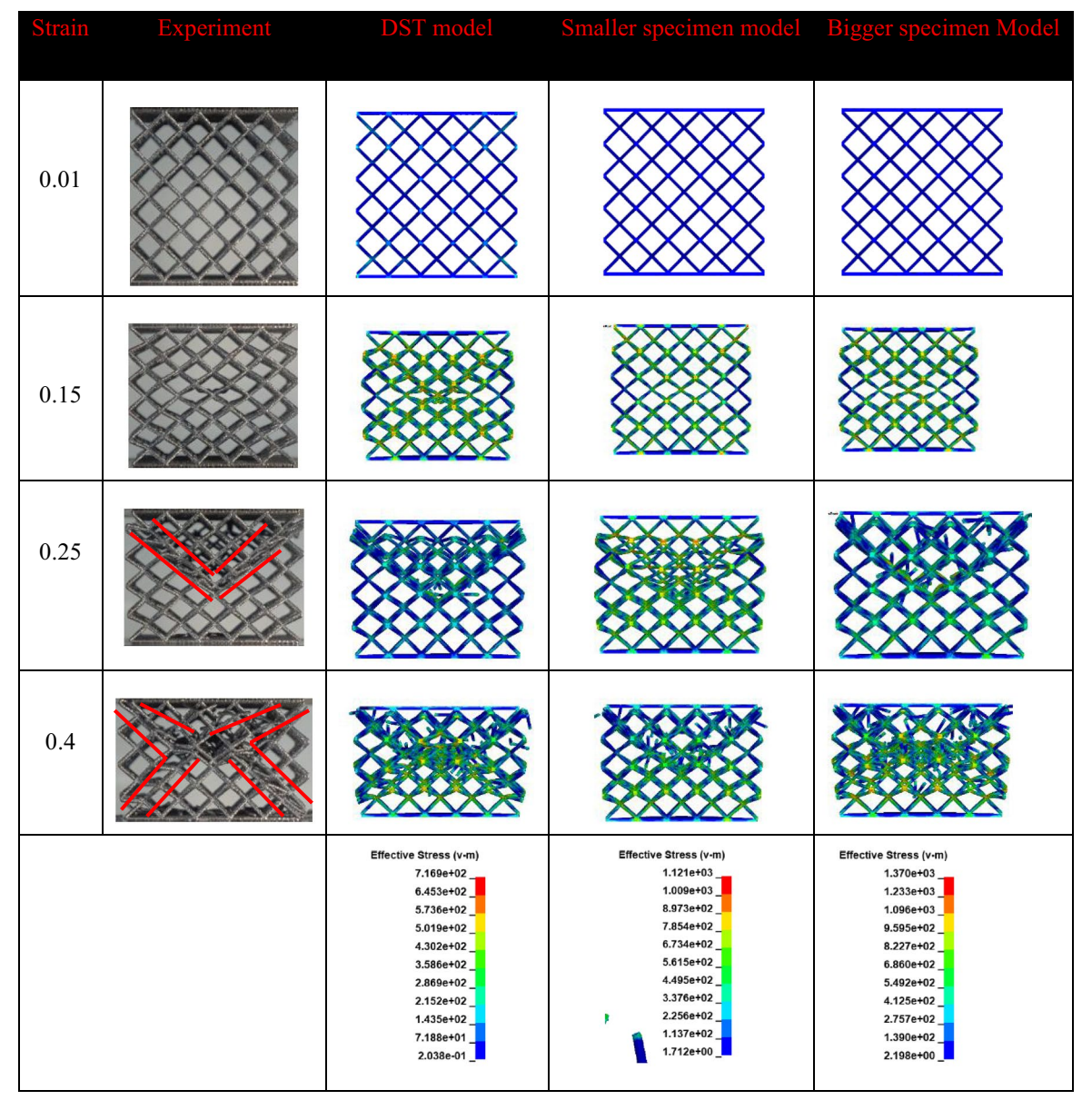
and their difference with the experiments are tabulated in Table 1. The DST verified model shows a 7% difference with the first peak stress as compared to 22.4% and 28.5% of the smaller and larger bulk JC models, respectively. The differences in densification strain ε_D and energy absorbed (EA) of DST and experiments are also the smallest as shown in Fig. 9.

To view how the specimen is shearing is also important as it affects the equivalent stress. Figure 10 shows the numerical DST deformation profile of the strut. The strut shows perfect (pure) shear from both sides with a relatively brittle failure. The strut shears at both sides simultaneously. Table 2 compares the experimental and numerical deformation pictures of the BCC lattice compression at different strains (%). Despite the differences in the stress values, each model shows a good match to the experiments in the deformation/ crushing profile which can be due to the similar damage parameters as dictated by the JC model. A strut diagonal shearing (V-shape) prevails initially and then followed by the X-shape which can be seen in both experiments and numerical simulations. Inside the formed shear bands, the broken struts are seen, proving the brittle type of the failures of the studied BCC lattices.

An interesting thing to note here is that even though the material, printing conditions, apparatus and powder sizes were similar, a difference in the constitutive equation was seen going from larger bulk samples to 1 mm. The results shown here are backed by several studies proving that the flow stress of a material changes when the thickness of the



 Table 2
 Deformation profile comparison of different models to the experiments



thin-walled strut is decreased but the failure pattern remains similar as also seen in Fig. 7b where the A and B values have effectively reduced [30]. It is also an understandable fact that the effect of stress decrease on a 1 mm strut would be higher than that of the bulk dog-bone sample because of the irregularities on the surface of EBM built samples are in the range of 150–300 μ m which effectively is a significant portion of the 1 mm strut structure.

The present results also show that compressing the asprinted strut specimens well estimates the flow stress behavior of the BCC lattices. This is further verified with the DST and DST numerical models. A further model parameter adjustment can also be made by the iterations of the flow stress parameters using the DST model in the numerical

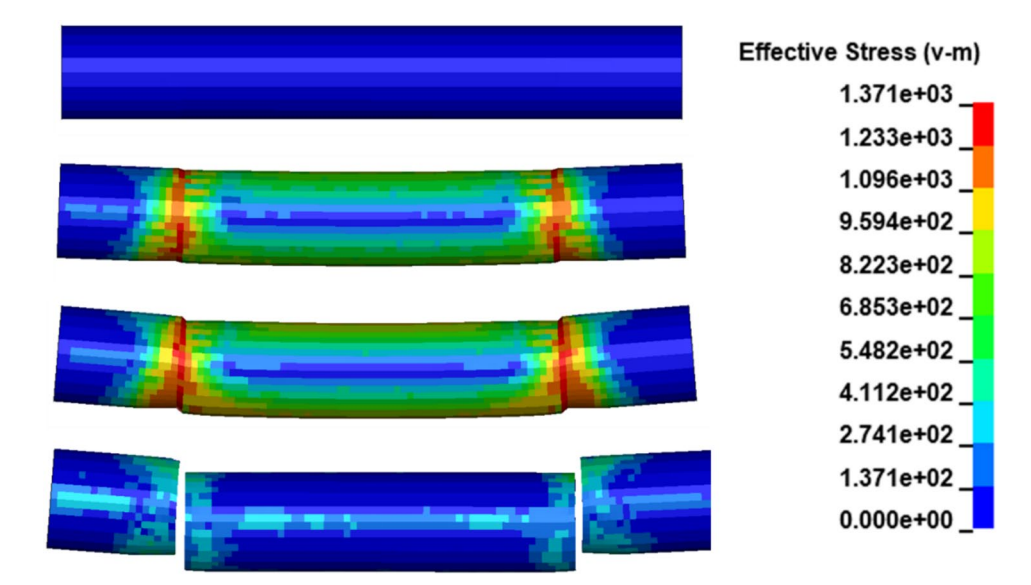
software. It should also be noted that the compression testing of struts may be difficult for very small diameter struts (1.5 mm height and 0.5 mm radius). In this case, the results of the DST can be iterated for the parameter that provides a best match to the experimental force—displacement curves of the DST.

5 Conclusions

A novel approach that combined the strut compression test, the strut DST and the numerical model of the strut DST using the JC equation was proposed. The approach



Fig. 10 Strut deformation in DST at different times till shear failure (Von-Mises stress profiles)



eliminated the use of bulk test specimens to extract the flow stress behavior of the BCC lattices under compression. The following were concluded:

The flow stresses determined from the machined bulk tension test specimens overestimated the BCC lattice compression stress–strain behavior. This was ascribed to the size-dependent mechanical response of the EBM specimens.

- Compression testing the as-printed strut specimens, on the other hand, showed the best estimation of the flow stress behavior of the compression tested BCC lattice which was also verified with the experimental and numerical DST.
- The DST numerical model and the experimental test results could be used for fine-tuning the flow stress model parameters through numerical iterations.

Supplementary Information The online version contains supplementary material available at https://doi.org/10.1007/s40964-025-01354-4.

Author contributions M.A.B.R.: drafting, design, formal analysis of the work, conducting experiments and data assembly. H.I.E.: solving errors in the numerical simulations, writing and editing the details of the Numerical study section. M.G.: supervision, design, conceptualization of the apparatus used, critical revision, final approval.

Funding H2020 Marie Skłodowska-Curie Actions, 101034425, Türkiye Bilimsel ve Teknolojik Araştırma Kurumu, 120C158,2236/B.

Data availability No datasets were generated or analyzed during the current study.

Declarations

Conflict of interests The authors declare no competing interests.

References

- Calignano F (2020) Additive manufacturing (AM) of metallic alloys. Crystals. https://doi.org/10.3390/cryst10080704
- Ao N et al (2018) Face-centered titanium induced by ultrasonic surface rolling process in Ti-6Al-4V alloy and its tensile behavior. Mater Charact 145:527–533
- Miracle DB et al (2001) ASM handbook, Vol. 21. ASM International Materials Park, OH.
- Nguyen HD et al (2022) A critical review on additive manufacturing of Ti-6Al-4V alloy: microstructure and mechanical properties. J Mater Res Technol 18:4641–4661
- Riaz MAB, Güden M (2025) A review of the experimental and numerical studies on the compression behavior of the additively produced metallic lattice structures at high and low strain rates. Def Technol. https://doi.org/10.1016/j.dt.2025.01.003
- Yan C et al (2021) Chapter 3—Metal alloys uniform TPMS structures. In: Yan C et al (eds) Triply periodic minimal surface lattices additively manufactured by selective laser melting, Academic Press, pp 39–130.
- Maconachie T et al (2019) SLM lattice structures: properties, performance, applications and challenges. Mater Des 183:108137
- Sun W et al (2020) Effects of build direction on tensile and fatigue performance of selective laser melting Ti6Al4V titanium alloy. Int J Fatigue 130:105260
- Jing S et al (2023) Enhancing mechanical properties of 3D printing metallic lattice structure inspired by Bambusa Emeiensis. Materials. https://doi.org/10.3390/ma16072545
- McDonnell B et al (2024) Bi-metallic lattice structures manufactured via an intralayer multi-material powder bed fusion method. Addit Manuf 89:104301



- Lozanovski B et al (2019) Computational modelling of strut defects in SLM manufactured lattice structures. Mater Des 171:107671
- Liu L et al (2017) Elastic and failure response of imperfect three-dimensional metallic lattices: the role of geometric defects induced by selective laser melting. J Mech Phys Solids 107:160-184
- Tancogne-Dejean T, Spierings AB, Mohr D (2016) Additivelymanufactured metallic micro-lattice materials for high specific energy absorption under static and dynamic loading. Acta Mater 116:14–28
- Güden M et al (2023) Investigation and validation of the flow stress equation and damage model parameters of an electron beam melted Ti6Al4V alloy with a martensitic phase. Mater Sci Eng A 885:145590
- Gümrük R, Mines R, Karadeniz S (2018) Determination of strain rate sensitivity of micro-struts manufactured using the selective laser melting method. J Mater Eng Perform 27:1016–1032
- Dressler AD et al (2019) Heterogeneities dominate mechanical performance of additively manufactured metal lattice struts. Addit Manuf 28:692–703
- Betts C, Balint D, Lin J (2014) In-situ micro-tensile testing and X-ray micro-tomography based FE modeling of open-cell metal foam struts and sandwich panels. Procedia Mater Sci 4:197–202
- Amani Y et al (2020) Micro-tensile behavior of struts extracted from an aluminum foam. Mater Charact 166:110456
- Ejeh CJ et al (2023) Combining multiple lattice-topology functional grading strategies for enhancing the dynamic compressive behavior of TPMS-based metamaterials. J Mater Res Technol 27:6076–6093
- Glema A, Łodygowski T, Sumelka W (2010) Nowacki's double shear test in the framework of the anisotropic thermo-elasto-vicsoplastic material model. J Theor Appl Mech 48:973–1001
- Jouri WS, Jones N (1988) The impact behaviour of aluminium alloy and mild steel double-shear specimens. Int J Mech Sci 30(3):153–172
- Meyer LW, Halle T (2011) Shear strength and shear failure, overview of testing and behavior of ductile metals. Mech Time-Depend Mater 15(4):327–340

- Rusinek A, Klepaczko JR (2001) Shear testing of a sheet steel at wide range of strain rates and a constitutive relation with strainrate and temperature dependence of the flow stress. Int J Plast 17(1):87–115
- Johnson GR, Cook WH (1983) A constitutive model and data for materials subjected to large strains, high strain rates, and high temperatures. In: Proceedings of 7th International Symposium on Ballistics, The Hague, 19–21 April 1983, pp. 541–547.
- Johnson GR, Cook WH (1985) Fracture characteristics of three metals subjected to various strains, strain rates, temperatures and pressures. Eng Fract Mech 21(1):31–48
- Smith CJ et al (2016) Dimensional accuracy of electron beam melting (EBM) additive manufacture with regard to weight optimized truss structures. J Mater Process Technol 229:128–138
- Inglis CE (1913) Stresses in plates due to the presence of cracks and sharp corners. Trans Inst Naval Architects 55:219–241
- Persson BNJ (2023) Surface roughness-induced stress concentration. Tribol Lett 71(2):66
- Ginestra P et al (2020) Selective laser melting and electron beam melting of Ti6Al4V for orthopedic applications: a comparative study on the applied building direction. Materials. https://doi.org/ 10.3390/ma13235584
- Majeed A et al (2023) Comprehensive mechanical behavior of thin-walled additively-manufactured parts of AlSi10Mg by SLM in as-built, post-solution, and aging treatment conditions. JOM 75(8):3067–3082

Publisher's Note Springer Nature remains neutral with regard to jurisdictional claims in published maps and institutional affiliations.

Springer Nature or its licensor (e.g. a society or other partner) holds exclusive rights to this article under a publishing agreement with the author(s) or other rightsholder(s); author self-archiving of the accepted manuscript version of this article is solely governed by the terms of such publishing agreement and applicable law.

